frontiers in Materials

ORIGINAL RESEARCH
published: 25 May 2021
doi: 10.3389/fmats.2021.665033

Insights Into the Microstructure and Dielectric Properties of Cold Sintered $NaCa_2Mg_2V_3O_{12}$ Based Composites

*Rakhi Madhuri, Santha Narayana Iyer and Subodh Ganesanpotti**

Department of Physics, University of Kerala, Kerala, India

Cold sintering process (CSP) was successfully employed to fabricate (1 − *x*) $NaCa_2Mg_2V_3O_{12}$-xNaCl [abbreviated as (1 − *x*) NCMVO-xNaCl] microwave dielectric ceramics. (1 − *x*)NCMVO-xNaCl ceramics prepared at 200°C and at a pressure of 450 MPa had a high relative density of 80–94%. X-ray diffraction (XRD), scanning electron microscope (SEM), energy dispersive X-ray spectroscopy (EDS), and Raman spectroscopy showed that both NCMVO and NaCl phases co-exist in all composite ceramics without forming any secondary phase. Further, dependence of microstructure and dielectric properties on cold sintering temperature and duration were investigated in detail and their optimized values to obtain maximum density of ceramic composites were 200°C and 50 min, respectively. (1 − *x*)NCMVO-xNaCl (x = 0.4–0.7) composites have relative permittivity (ε_r) in the range of 6.9–7.4, and a reasonably high microwave quality factor (Q × f) of 5,000 to 13,830 GHz.

Keywords: cold sintering process, relative permittivity, garnet, NaCl, microwave dielectric properties

OPEN ACCESS

Edited by:
Mailadil Thomas Sebastian, University of Oulu, Finland

Reviewed by:
Changzheng Hu, Guilin University of Technology, China
Di Zhou, Xi'an Jiaotong University, China

****Correspondence:***
Subodh Ganesanpotti
gsubodh@gmail.com

Specialty section:
This article was submitted to Ceramics and Glass, a section of the journal Frontiers in Materials

Received: *06 February 2021*
Accepted: *19 April 2021*
Published: *25 May 2021*

Citation:
Madhuri R, Narayana Iyer S and Ganesanpotti S (2021) Insights Into the Microstructure and Dielectric Properties of Cold Sintered $NaCa_2Mg_2V_3O_{12}$ Based Composites. Front. Mater. 8:665033. doi: 10.3389/fmats.2021.665033

INTRODUCTION

The microwave dielectric ceramics are the fundamental building units of different multifunctional devices, which are widely used for communication purposes such as oscillators, substrates, resonator antennas, filters, radomes, and multilayer packages (Cava, 2001; Reaney and Iddles, 2006; Zhou et al., 2018). The rapid evolution from 4G to 5G technologies enables newly developed devices with fast signal response performance (Fiedziuszko et al., 2002; Ohsato, 2012; Sebastian et al., 2015; Faouri et al., 2019; Ji et al., 2019). However, the stringent requirements for the signal propagation are very low relative permittivity in order to increase the signal propagation speed, low dielectric loss to achieve better selectivity as well as speed of device, near zero temperature coefficient of resonant frequency for reliable operation and low thermal expansion in order to work in harsh environmental situations. The materials for these applications are in the form of resonators and substrates such as HTCCs, ULTCCs, and PCBs. Recently LTCC and ULTCC get more attention because of its compatibility with inexpensive electrodes such as Ag/Al/Cu. However, there exist problems between LTCC/ULTCC and electrodes including delamination, formation of parasitic phases and inter diffusion, which prompt the researchers to develop another technology for fabrication of multilayer devices for communication purposes (Green et al., 2008; Zhou et al., 2011; Guo et al., 2014a).

The cold sintering process (CSP) has recently emerged as fast, energy efficient, and low cost technology to develop dense ceramics, polymers, ceramic composites, etc. The cold sintering method is realized under appropriate uniaxial pressure (100–500 MPa) with low temperatures

(<300°C) and short time periods (≤1 h), which uses water as a transient solvent. In the conventional solid state sintering technology solid state diffusion takes place while the CSP occurs at a solid–liquid interface (Kahari et al., 2014; Guo et al., 2016, 2017, 2014b; Kähäri et al., 2016; Induja and Sebastian, 2017; Randall et al., 2017; Väätäjä et al., 2017, 2018; Wang et al., 2019a). Even though the basic theories involved in CSP are developed, the exact mechanisms involved are yet to emerge. The first report on fundamental mechanisms involved in cold sintering technique, which is a two stage process, was suggested by Maria et al. (2017). During the first stage of CSP, the powder in the die prompts particle rearrangement under a uniaxial pressure with the help of solvent. As temperature increases from 100 to 300°C, the solid forms a dense ceramic by a dissolution-precipitation mechanism (Wang et al., 2021). Bouville and Studart (2017) reported that when the pressure increases above 100 MPa in CSP, a phenomenon named as plastic deformation happens and is demonstrated by Hong et al. (2018) in their experiment on cold sintering of NaCl. Kähäri et al. (2016) reported that Li_2MoO_4 ceramics could be densified at room temperature by the addition of water as solvent and using uniaxial pressure. They reported that its density and dielectric properties are same as that of conventionally sintered one. This technique is successfully applied to many ceramics, ceramic composites and polymers such as LMO, $Na_2Mo_2O_7$, $K_2Mo_2O_7$, $Li_{0.5}Bi_{0.5}MoO_4$, LMO-PTFE (Väätäjä et al., 2017), and $CaTiO_3$ (CTO)-KMO (Wang et al., 2020). Wang et al. (2018b, 2019a) reported a novel dielectric GRIN lens based on the cold sintering of NBMO-xLMO and BLVMO-xNMO systems. Moreover CSP has attracted a lot of research interest in a wide range of areas especially in the field of semiconductors, ionic conductors, piezoelectric ceramics, Li ion batteries, nano composites, thermo electrics and low dielectric loss ceramics (Berbano et al., 2017; Funahashi et al., 2017a; Seo et al., 2017; Charoonsuk et al., 2018; Gonzalez-Julian et al., 2018; Induja and Sebastian, 2018; Leng et al., 2018; Ndayishimiye et al., 2018a,b; Wang et al., 2018a; Sibi et al., 2020). Induja and Sebastian (2018) reported that Al_2SiO_5 ceramics can be easily densified using CSP with the aid of NaCl as water soluble additive. Sibi et al. (2020) found that garnet mineral can be densified using NaCl, Li_2MoO_4, and V_2O_5. Recently, Santha et al. (2020) reported the dielectric properties of cold sintered $MgTiO_3$ using NaCl as additive. Besides the advantages of low temperature, CSP can produce a near shape pellets, having the same diameter of the model and also there occurs no reaction between the ingredients, which paved the way to integrate the polymers, composites, nano particles and metals in ceramic matrix composites. Moreover, Lee et al. (2019) reported the electrochemical properties of ceramic–salt composite electrolytes prepared by CSP. The first microstrip patch antenna was designed and fabricated using a cold sintered LMO substrate (Kahari et al., 2017). Recently, Reaney et al. developed a cold sintered CoG multilayer capacitor with Ag internal electrodes (Wang et al., 2019b). All these studies give insight into the effect of CSP on proper densification of ceramic, ceramic–polymer composites and also its practical importance in microwave industries.

The vanadate based garnet systems are widely investigated for low dielectric loss and relatively lower relative permittivity. The garnet systems have the general composition $A_3B_2C_3O_{12}$, which have three different sites (A, B, and C) for a wide variety of cation substitutions. The C ions form CO_4 tetrahedra, while the B-site ions form octahedral coordination with the oxygen atoms. The corner-shared octahedra and tetrahedra form dodecahedra, where the A-site ions are placed (Rakhi and Subodh, 2020). Among this, Fang et al. studied dielectric

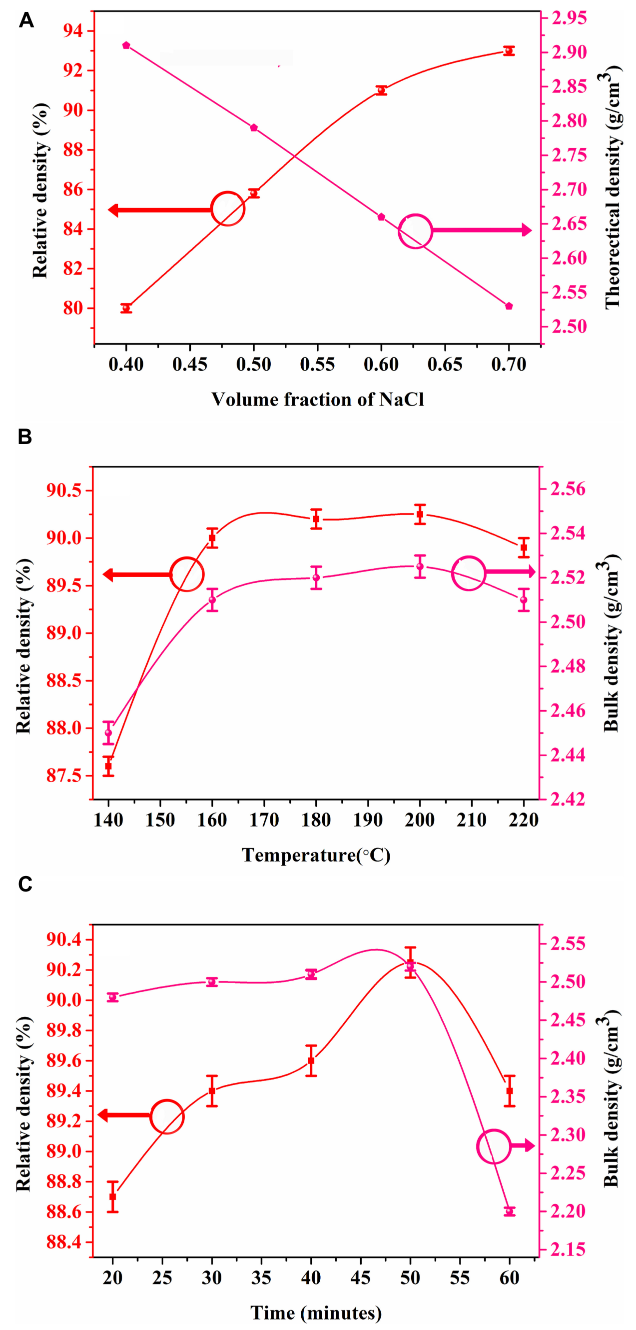

FIGURE 1 | Dependence of Bulk density and relative density of (1 – *x*)NCMVO-xNaCl composite with **(A)** volume fraction of NaCl, **(B)** temperature, and **(C)** time.

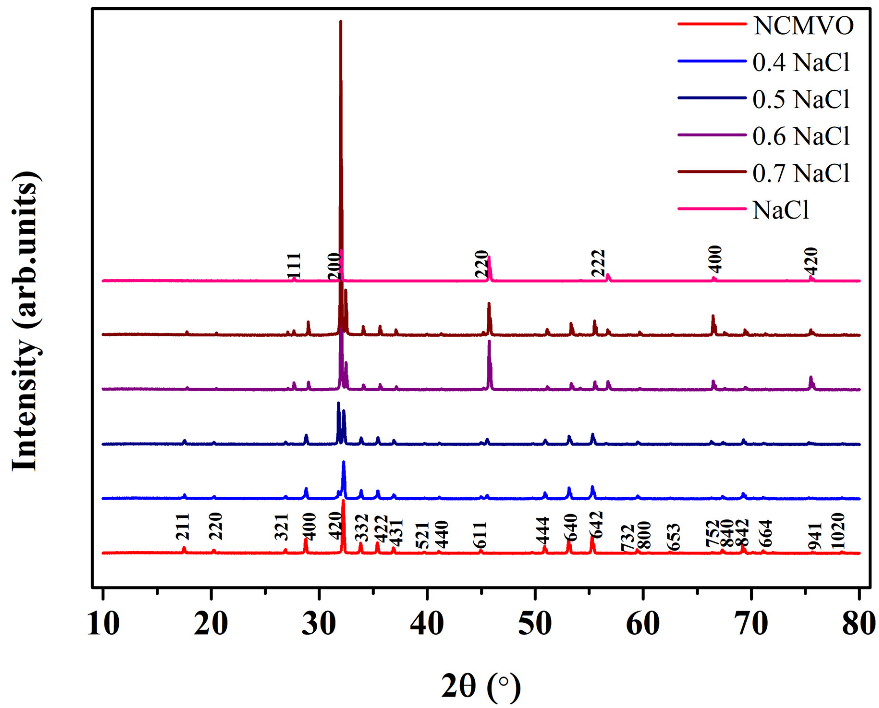

FIGURE 2 | The X-ray diffraction patterns of NCMVO, NaCl and (1 – *x*) NCMVO-x NaCl (*x* = 0.4, 0.5, 0.6, and 0.7) composites.

properties of $NaCa_2Mg_2V_3O_{12}$ ceramic, which possesses relative permittivity of 10, quality factor around 50,600 GHz and temperature coefficient of resonant frequency of −47 ppm/°C (Fang et al., 2013). To the best of our knowledge, there are no reports on cold sintered vanadate garnet systems for future microwave applications. In this work NCMVO and NaCl were selected to fabricate $(1 - x)$NCMVO-xNaCl (x = 0.4, 0.5, 0.6, and 0.7) ceramic composites by CSP to show the possibility of fabricating dense garnet system ≤200°C. The influence of time and temperature on its microstructure and microwave dielectric properties is also studied.

EXPERIMENTAL SECTION

$(1 - x)NaCa_2Mg_2V_3O_{12}$-xNaCl ($x$ = 0.4, 0.5, 0.6, and 0.7) ceramic composites [$(1 - x)$ NCMVO-xNaCl] were prepared through cold sintering technique. The NCMVO ceramics were prepared through conventional solid state reaction method. Raw materials such as Na_2CO_3 (Sigma Aldrich ≥ 99.5%), $CaCO_3$ (Alfa aesar ≥ 99.5%), MgO (Sigma Aldrich ≥ 99.0%), and NH_4VO_3 (Sigma Aldrich ≥ 99.0%) were weighed stoichiometrically according to the composition and ball milled using acetone medium for 24 h. Then the dried and ground powders were calcined at 800°C /4 h. To prepare [$(1 - x)$ NCMVO-xNaCl] composites, the calcined NCMVO were mixed with different volume fractions of NaCl (Alfa aesar > 99.99%) powder with the addition of 10–15 wt% deionized water. Then the mixture was hot pressed at temperatures ranging from 140 to 220°C for a period of 20–60 min under a constant pressure of 450 MPa. Then the pressed pellets were dried in an oven for 24 h at 120°C in-order to remove residual moisture content.

The bulk densities of the samples were obtained using geometric method. The phase purity and crystal structure of the synthesized compounds were investigated by X-ray diffraction (XRD) using CuKα radiation (λ = 1.5406 Å) in a Bruker D8

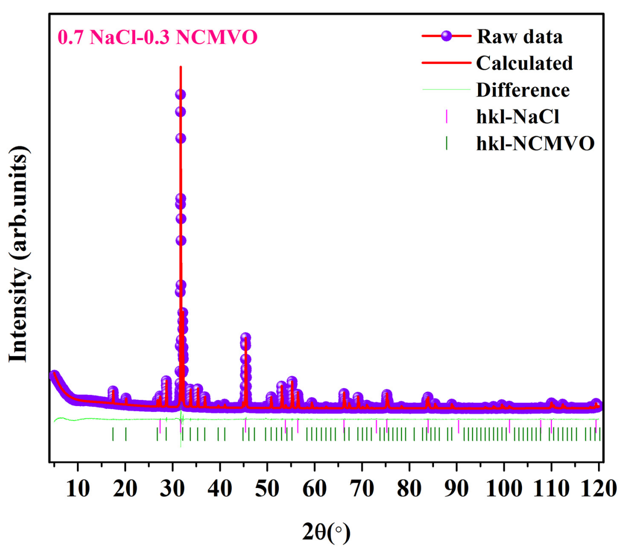

FIGURE 3 | Rietveld refinement analysis of 0.3NCMVO-0.7 NaCl composite ceramic using the TOPAS 4.2 package.

Advance Diffractometer. The room temperature Raman spectra were recorded using a HORIBA Raman spectrometer with excitation wavelength of 532 nm in the spectral range from 100 to 1,000 cm^{-1}. The surface morphology of the compounds was analyzed using a scanning electron microscope (SEM) (ZEISS EVO 18). The broadband dielectric response in the frequency range of 1 MHz to 1 GHz was analyzed using a Keysight E4991B impedance analyzer with a 16,453A dielectric test fixture. The microwave dielectric properties were measured using a vector network analyzer (ROHDE and SCHWARZ, ZV-Z135). The $TE_{01\delta}$ mode cavity method was used to measure the relative permittivity and unloaded quality factor of the compounds. The temperature coefficient of the resonant frequency (τ_f) was found out by noting the variations in the $TE_{01\delta}$ mode frequency having temperature range from 25 to 85°C, using the following formula:

$$\tau_f = \frac{f_{85} - f_{25}}{60 \times f_{25}} \times 10^6 \text{ ppm/°C}$$

where f_{25} and f_{85} are the resonant frequencies at 25 and 85°C, respectively.

RESULTS AND DISCUSSION

Density Analysis

Figure 1A shows the theoretical densities and relative densities of $(1 - x)$ NCMVO-xNaCl ceramic composites with increase in volume fraction of NaCl. **Figures 1B,C** shows the variation of density with temperature and time for 0.5NCMVO–0.5NaCl. As the concentration of NaCl increases, the theoretical density of the composite decreases linearly, due to the lower density of NaCl compared to NCMVO (2.16 g/cm^3 for NaCl and 3.42 g/cm^3 for NCMVO). The relative densities of all the $(1 - x)$ NCMVO-xNaCl ceramic composites are in the range of 80–94% of theoretical density. As the volume fraction of NaCl increases the relative density increases, which confirms that the ceramic material can be densified with NaCl having a solubility of 359 Kg/m^3. Temperature and time also play important roles for dissolution of soluble additives. Hence the effect of temperature and time at constant pressure in the transport of particles to the pores is also studied. For 0.5 NCMVO–0.5 NaCl composite, density increases from 85 to 90% as temperature increases from 140 to 200°C, thereafter

TABLE 1 | Refined Structural Parameters of NCMVO- NaCl Composite Ceramic.

Composition	Lattice parameter (Å)	R_{WP} (%)	R_P (%)	GOF	Phase fraction (%)
0.7 NaCl-0.3 NCMVO	*a* = 12.4363(8)	5.1	6.7	2.3	NaCl = 65.08
	a = 5.6409 (9)				NCMVO = 34.92
0.5 NaCl-0.5 NCMVO	*a* = 12.4329(5)	6.62	5.11	1.44	NaCl = 36.96
	a = 5.6418(8)				NCMVO = 63.04

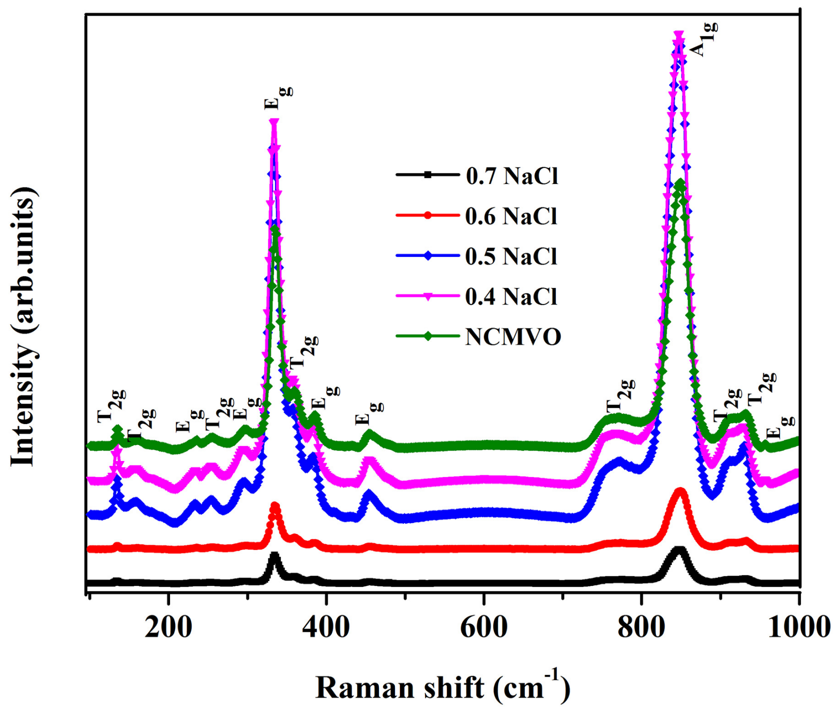

FIGURE 4 | The Raman spectra of NCMVO and (1 – *x*) NCMVO-xNaCl (*x* = 0.4, 0.5, 0.6, and 0.7) composites.

it shows a slight decrease, which may be due to the rapid evaporation of water at higher cold sintering temperature, giving rise to the incomplete dissolution precipitation. In order to study the variation of density with time of 0.5 NCMVO–0.5 NaCl composite, the temperature was fixed as 200°C and the time was varied from 20 to 60 min. The density of the composite increased as time increased from 20 to 50 min and there after it showed a slight decrease. During the preliminary stage of cold sintering, particle rearrangement takes place through the liquid medium. The second stage is associated with the dissolution of particles with the presence of pressure and temperature, which leads to the development of a supersaturated phase, followed by nucleation and densification of the ceramic composites (Yu et al., 2019; Wang et al., 2021). Hence optimum time and temperature are necessary for proper densification of composites by cold sintering.

X-ray Diffraction Analysis

Figure 2 shows the room temperature XRD patterns of $(1-x)$ NCMVO-xNaCl (x = 0.4, 0.5, 0.6, and 0.7) ceramic composites along with that of NCMVO and NaCl. NCMVO crystallizes in the cubic garnet structure with space group Ia/3d (ICDD PDF No. 01-072-3824). In the garnet structure of NCMVO, Na^+, and Ca^{2+} atoms occupy the 24*c* Wyckoff position, where they form dodecahedral coordination with eight oxygen atoms. The Mg^{2+} atoms are situated in the 16*a* sites having octahedral point symmetry (S_6) and the V^{5+} atoms are positioned in the 24*d* site with tetrahedral point symmetry (S_4) and the oxygen atoms located in the 96 h wyckoff site. NaCl crystallizes in the cubic system with space group Fm-3m (225) (ICDD PDF No. 00-005-0628).The intensity of NaCl diffraction peaks in the XRD pattern increases with increase in the volume fraction of NaCl. Diffraction peaks corresponding to only NCMVO and NaCl are present indicating that there is no chemical reaction between NCMVO and NaCl. The Rietveld refinements of the composites 0.3NCMVO-0.7NaCl and 0.5 NaCl-0.5 NCMVO were also performed using the TOPAS 4.2 software, where a two phase refinement (Ia$\bar{3}$d +Fm-3m) was used. **Figure 3** and **Supplementary Figure 1** shows the Rietveld refined pattern of 0.7 NaCl-0.3NCMVO and 0.5 NCMVO-0.5NaCl composites. For the volume fraction of 0.3 NCMVO-0.7 NaCl (40 and 60 wt%, respectively) and 0.5 NaCl-0.5 NCMVO (35 and 65 wt%, respectively) the weight fraction obtained after refinement is close to the nominal composition and is given in the **Table 1**.

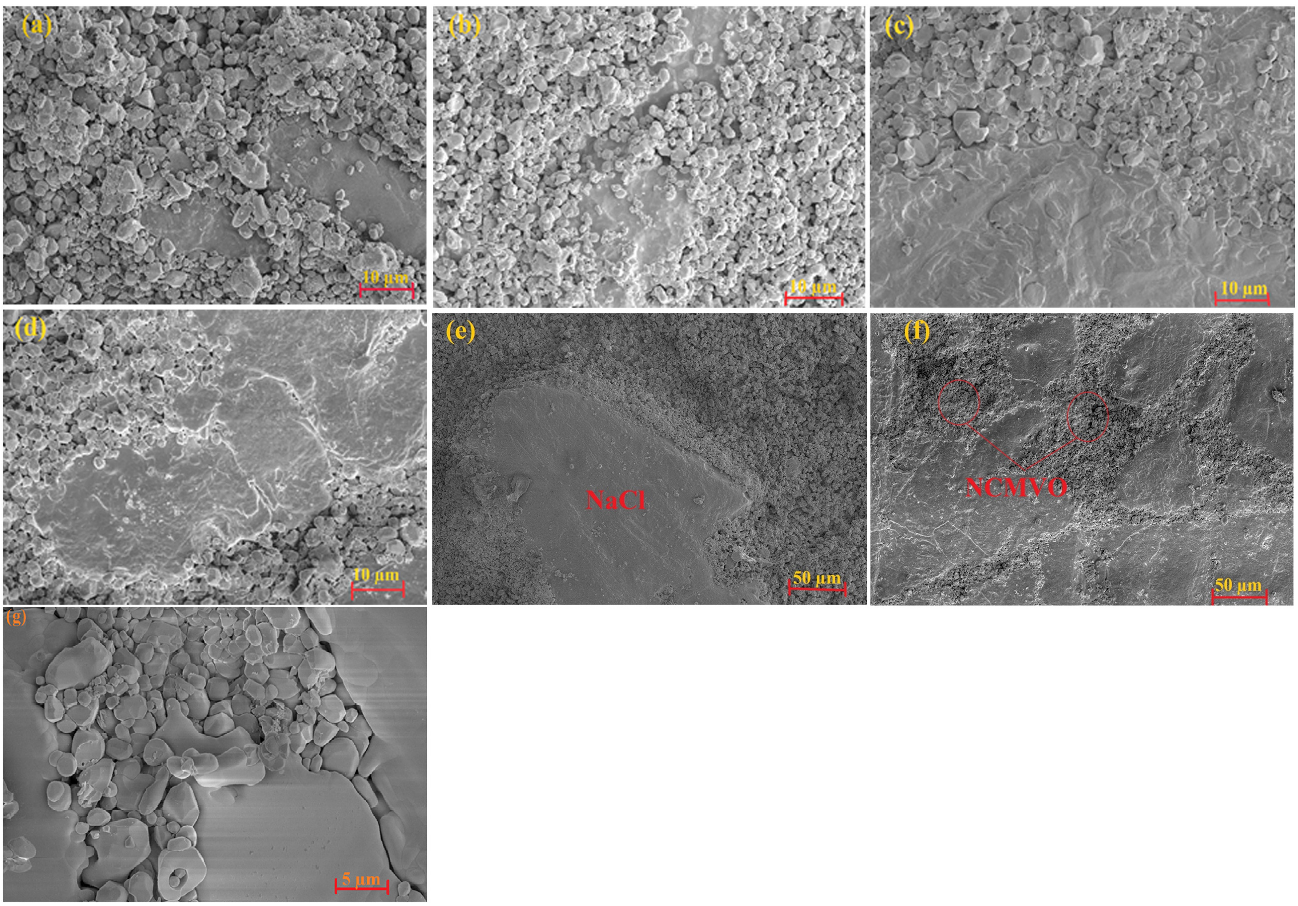

FIGURE 5 | The microstructure of $(1-x)$ NCMVO-xNaCl **(a,e)** x = 0.4 NaCl, **(b)** x = 0.5, **(c)** x = 0.6, and **(d,f)** x = 0.7, and **(g)** fractured surface of 0.5 NaCl–0.5 NCMVO composites.

Raman Analysis

Figure 4 shows the Raman spectra of (1 − *x*) NCMVO-xNaCl (*x* = 0.4, 0.5, 0.6, and 0.7) composites. The group theory predicts that for a garnet structure at the Brillouin zone center, 98 vibrational modes exist, in which 55 are silent modes and one is acoustic in nature. The remaining are 17 IR-active and 25 Raman-active vibrations.

$$\Gamma_{total} = 3A_{1g} + 5A_{2g} + 8E_g + 14T_{1g} + 14T_{2g}$$
$$+5A_{1u} + 5A_{2u}10 + E_u + 18T_{1u} + 16T_{2u}$$
$$\Gamma_{acoustic} = T_{1u}$$

The 25 Raman active bands are $3A_{1g}$+$8E_g$+$14T_{2g}$, whereA_{1g},E_g, and T_{2g}correspond to the internal modes, translational modes and rotatory modes, respectively. In a garnet system, the Raman-active vibrations are divided into external and internal modes. The translational motion of the cations are responsible for external modes, and the internal vibrations are associated with the vibrations of the $(VO_4)^{3-}$ tetrahedra. The A_{1g} modes with maximum intensity correspond to the stretching and bending vibrations of the VO_4 group. The modes come below 250 cm^{-1} are generally associated with external translational motion of Na^+/Ca^+ and Mg^{2+}—O bonds. The internal bending vibrations of $(VO_4)^{3-}$ lie between 300 and 600 cm^{-1}, whereas the modes above 600 cm^{-1} represent the symmetric and asymmetric stretching vibrations of the $(VO_4)^{3-}$group, which linearly depend on the lattice parameter values (Koningstein and Mortensen, 1968; Moore et al., 1971; White and Keramidas, 1971). NaCl has no Raman active bands in the range of 10–1,000 cm^{-1}.

Microstructure and Elemental Analysis

Generally microstructure is used to confirm the densification of a sample and to study its influence on the physical properties of system. **Figures 5a–g** shows the microstructure of (1 − *x*) NCMVO-xNaCl (*x* = 0.4, 0.5, 0.6, and 0.7) ceramic composites. From the microstructure, it is clear that only two discrete types of grains are present in all the compositions, which agrees with the

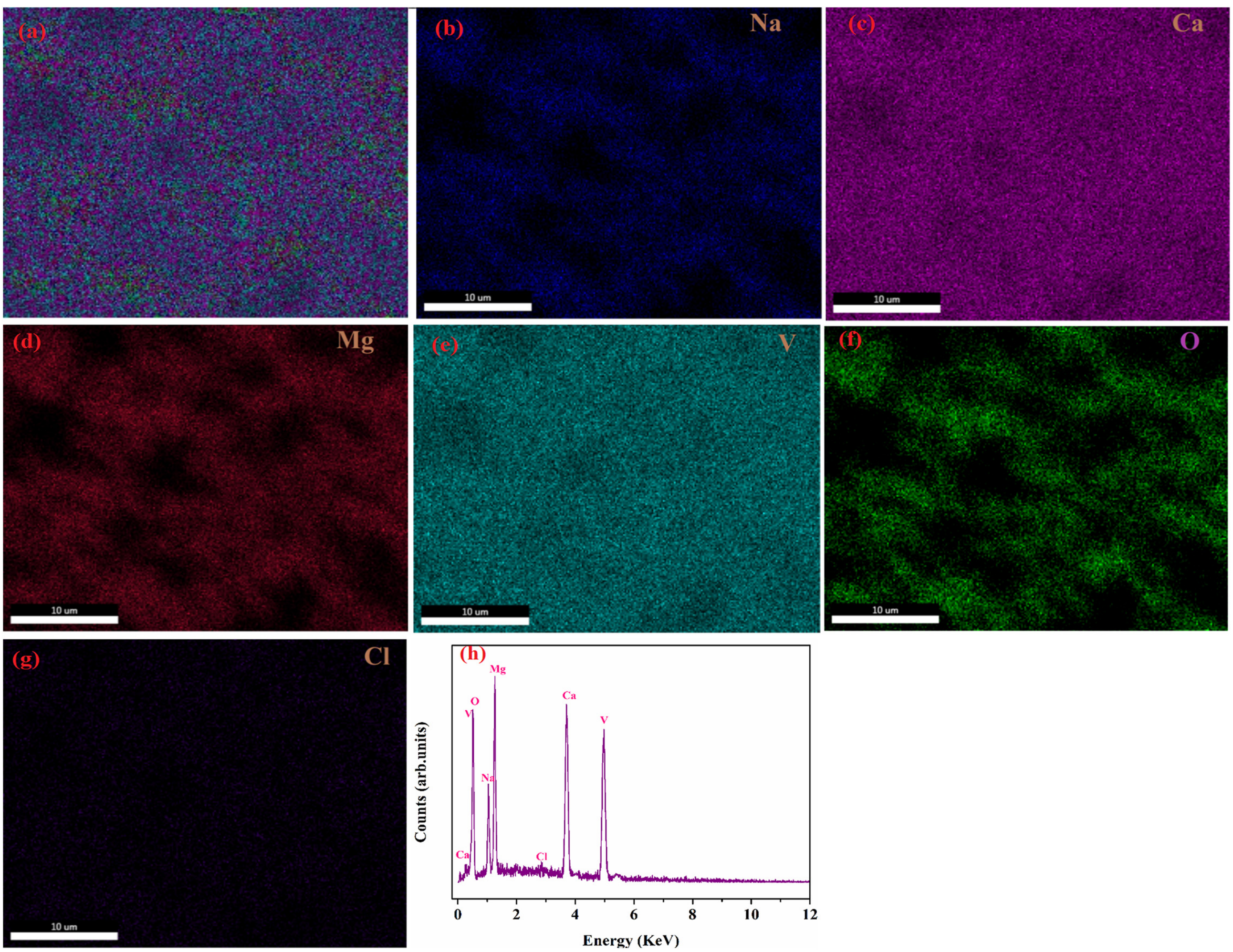

FIGURE 6 | EDS spectra and mapping of 0.5NCMVO-0.5NaCl composite with **(a)** EDS mapping of 0.5NCMVO-0.5NaCl composite; **(b)** Na; **(c)** Ca; **(d)** Mg; **(e)** V; **(f)** O; **(g)** Cl; and **(h)** EDS spectra of the 0.5NCMVO-0.5NaCl composites.

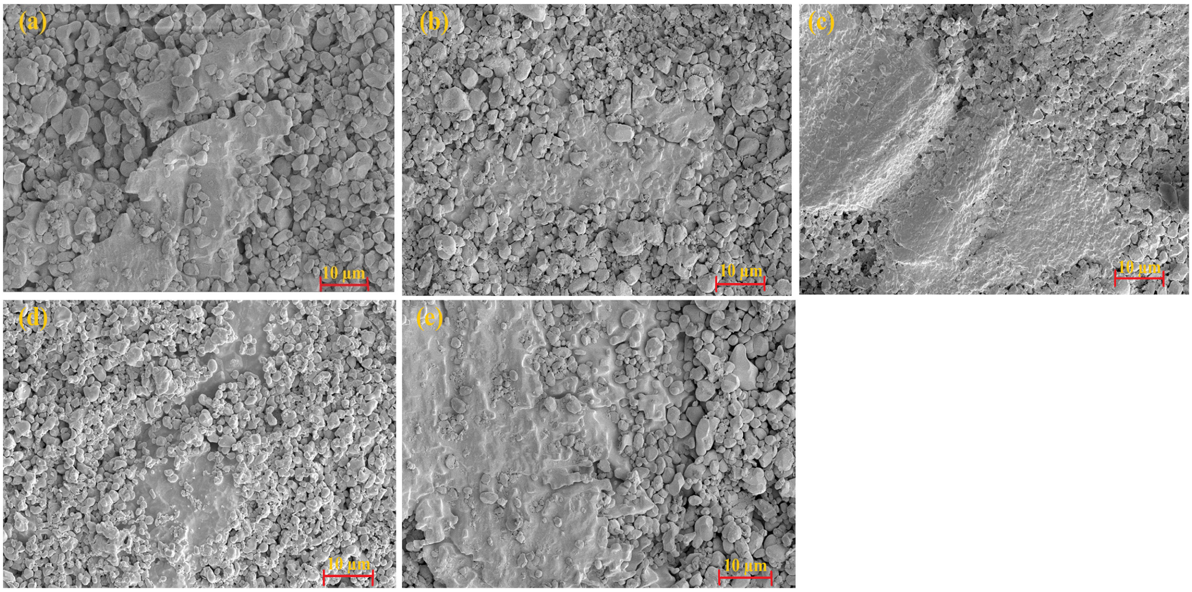

FIGURE 7 | Dependence of microstructure of 0.5NCMVO-0.5NaCl composite with sintering temperature **(a)** 140°C, **(b)** 160°C, **(c)** 180°C, **(d)** 200°C, and **(e)** 220°C.

XRD results. The large grain corresponds to NaCl and the small grains represent NCMVO having elements Na, Ca, Mg, V, and oxygen. For 0.4 volume fraction NaCl, composite shows a porous structure with densification around 78%. As the volume fraction of NaCl increases, the densities of composites also increase and obtain a maximum value of 94% for 0.7-volume fraction of NaCl, which is evident from the microstructures of the composites. The densification mechanisms in the cold sintering technique involves the dissolution of NaCl grains into the added water molecule under the aid of pressure, temperature and the capillary action of NCMVO grains. As the water evaporates, Na^+ and Cl^- ions crystallize on the surface of NaCl and NCMVO grains, which will result in the densification of NCMVO particles and NaCl grains. As the volume fraction of NaCl increases from 0.4 to 0.5 its grain size also increases, there after it can be noticed that bulk chuncks of NaCl are formed and NCMVO grains are occupied in between these bulk NaCl grains. The internal mechanism behind the grain growth was dissolution-precipitation process. In the microstructure of $(1-x)$ NCMVO-xNaCl composites, the garnet grains found to be scattered whereas NaCl grains form necks with each other as the volume fraction of NaCl increases, which enhances the grain size of NaCl compared to NCMVO. The enhancement in grain growth happened as a result of particle (NaCl) transportation from higher to lower chemical potential. Similar type of grain growth occurred in pure ZnO reported by Funahashi et al. (2017b) and also in garnet mineral reported by Sibi et al. (2020). **Figures 6a–h** shows the EDS mapping and spectra for the optimum volume fraction of 0.5 NCMVO-0.5 NaCl composite.

TABLE 2 | Variations of relative permittivity, quality factor and temperature coefficient of resonant frequency of $(1-x)$NCMVO-xNaCl composites at 200°C, 50 min.

$(1-x)$NCMVO-xNaCl	ε_r	Density (%)	Qu*f (GHz)	τ_f (ppm/°C)
0.4	6.1	80	4,784	−41
0.5	6.2	86	13,900	−47
0.6	6.6	91	10,300	−52
0.7	6.7	93	9,750	−112

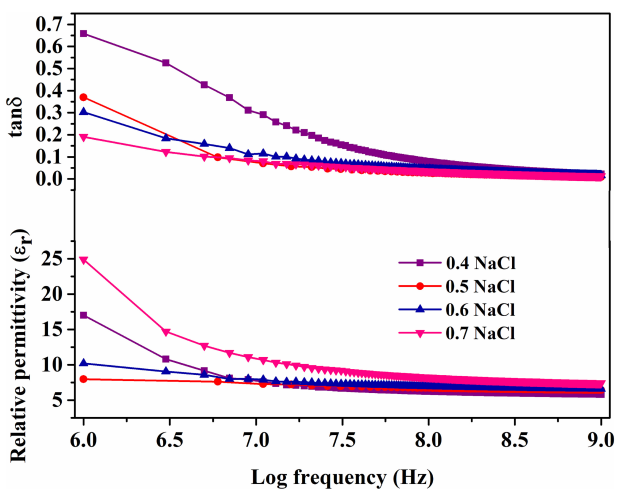

FIGURE 8 | Dependence of relative permittivity and tanδ with NaCl volume fraction.

Figures 7a–e show the variation of microstructure with temperature for 0.5-volume fraction of NaCl. As the temperature is increased, at a constant pressure of 450 MPa, density increases to 90% which is evident from microstructure. During the preliminary stage of CSP, due to the rearrangement of particles a supersaturated environment was developed. Thus for short cold sintering time and low cold sintering temperature, the particle rearrangement is not complete and it forms an agglomerated microstructure, and that influences the dielectric behavior of the system. As the temperature increases we can see more prominent grains and grain boundaries in the microstructure, which are well packed in its structure. So it is clear that for densifying garnet material through cold sintering technique, NaCl is one of the suitable additives and also the proper temperature and time are critical for the proper densification process.

Broad Band Dielectric Properties of Garnet Composite System

Figure 8 shows the broad band dielectric properties of $(1 - x)$ NCMVO-xNaCl (x = 0.4, 0.5, 0.6, and 0.7) composites. As the frequency increases, the relative permittivity and dielectric loss decrease due to the decrease in polarization. When the frequency increases, polarization mechanisms (dipolar, ionic, atomic, and electronic) present in the material decreases, resulting in the decrease in relative permittivity. As frequency increases only electronic polarization contributes to the net polarization and hence the material shows a decrease in relative permittivity. Beyond certain critical frequency, electrons inside the material cannot follow the alternating frequency of AC electric field, which results in the drop of dielectric loss as frequency increases. As the volume fraction of NaCl increases, the porosity corrected relative permittivity decreases, which may be due to the low relative permittivity of NaCl compared to NCMVO ceramics. When the volume fraction of NaCl increases from 0.4 to 0.7, the relative permittivity decreases from 8.1 to 7.3, while the dielectric loss also decreases, this may be due to the improvement in microstructure with higher volume fraction of NaCl.

Supplementary Figure 2 shows the variation of relative permittivity and dielectric loss of 0.5NCMVO-0.5NaCl at different temperatures. As the temperature increases, the relative permittivity shows slight increase due to the increased densification. The optimized temperature is found to be 200°C, at which the relative permittivity is about 6.4 and dielectric loss is in the range of 0.0089 at 1 GHz. The variation of relative permittivity with temperature is small, and ranges between 5.8 and 6.4. However the dielectric loss decreases with temperature and reaches a minimum value of 0.0089 at 200°C, due to the compact microstructure of composites.

TABLE 3 | A comparison of experimental and theoretical relative permittivity.

Volume fraction of NaCl	Relative permittivity (ε_r)			
	Measured value	Porosity corrected value	Lichtnecker's rule	Simple mixing rule
0.4	6.1	7.4	8.0	7.8
0.5	6.2	7.2	7.6	7.4
0.6	6.6	7.0	7.2	7.0
0.7	6.7	6.9	6.8	6.9

Supplementary Figure 3 shows the dependence of cold sintering time on dielectric properties of 0.5NCMVO-0.5NaCl composite. As the time increases, the relative permittivity is almost constant while the dielectric loss decreases with a minimum value at 50 min, which was taken as the optimum time for the cold sintering of $(1 - x)$NCMVO − xNaCl composites. For lower holding time the particle agglomeration, sharp edged grain and poor rearrangement of individual phases resulted in porous microstructure, which causes high dielectric loss. So for better microstructure and best dielectric properties optimum time of holding is necessary, which is found to be 50 min for NCMVO–NaCl composites.

Microwave Dielectric Properties

Table 2 shows the microwave dielectric properties of $(1 - x)$ NCMVO-xNaCl (x = 0.4, 0.5, 0.6, and 0.7) composites. As the volume fraction of NaCl increases the relative permittivity also increases, which may be due to the increasing density of the composites. So in order to find the correct trend we calculate the porosity corrected relative permittivity from measured one using the equation given by Bosman and Having as follows (Yoon et al., 2006)

$$\varepsilon_{\text{Bosman}} = \varepsilon_{\text{m}} (1 + 1.5P) \quad (1)$$

$$P = \left(1 - \frac{\rho_{\text{mea}}}{\rho_{\text{theo}}}\right) \quad (2)$$

where ε and ε_m are the porosity-corrected and measured relative permittivity, respectively. P is the fractional porosity. The porosity corrected relative permittivity of composites decreases as the volume fraction increases. For $(1 - x)$ NCMVO-xNaCl composites the relative permittivity comes in the range of 6–7. In ceramic composite systems, the relative permittivity of materials can determined by the permittivity of individual phases, its corresponding volume fraction and complex form of its component materials. Lichtnecker equation widely used for two phase ceramic systems is as follows:

$$\varepsilon^n = V_1 \varepsilon_1{}^n + V_2 \varepsilon_2{}^n (-1 < n < 1). \quad (3)$$

when n = 1 or −1 the above equation becomes parallel or series mixing law, respectively.

$$\varepsilon_c = V_1 \varepsilon_1 + V_2 \varepsilon_2 \quad (4)$$

$$\frac{1}{\varepsilon c} = \frac{V_1}{\varepsilon_1} + \frac{V_2}{\varepsilon_2} \quad (5)$$

where ε_c is the relative permittivity of NCMVO – NaCl composites. V_1 and V_2 are the volume fractions of NCMVO and NaCl, respectively, ε_1 and ε_2 are the corresponding relative permittivity.

For randomly distributed systems the equation become logarithmic as follows where n approaches zero.

$$ln\varepsilon_c = V_1 ln\varepsilon_1 + V_2 ln\varepsilon_2 \quad (6)$$

Table 3 gives the theoretical relative permittivity obtained using simple mixing rule and logarithmic rule. The relative permittivity of conventionally sintered NCMVO is about 10 and is used here for calculations due to the low density of cold sintered pure samples. Both intrinsic and extrinsic factors contribute to microwave dielectric loss. The microwave dielectric losses may due to substitution, impurity, secondary phases, cavity, oxygen vacancies, poor density, etc. In which the effect of grain sizes come under the category of extrinsic losses, while the losses arising from the variations occurring in lattice and crystal structure are come in the category of intrinsic dielectric losses. In the present case, even though $(1 - x)$ NCMVO-xNaCl (x = 0.4, 0.5, 0.6, and 0.7) composites show a higher density with increase in volume of NaCl, its $Q_u \times f$ is slightly lower beyond 0.5 volume fraction of NaCl, which could be due to decreased quality factor of NaCl compared with NCMVO ceramics. It was reported that cold sintered NaCl possess a quality factor in the range 12,000–49,600 GHz depending on the processing conditions, while that of NCMVO has a reported value of around 50,600 GHz (Hong et al., 2018; Wang et al., 2021; Fang et al., 2013). The quality factor of a two phase composite can be determined by

$$Q^{-1} = \mathrm{V}_1 Q_1^{-1} + \mathrm{V}_2 Q_2^{-1} \tag{7}$$

The terms Q, Q_1, and Q_2 represent the quality factor of the composite, and the two phases of composite with volume fraction V_1 and V_2, respectively. According to Equation (7), as the volume fraction of NaCl increases the quality factor should decrease. Measured values also show a similar trend except for 0.5 volume fraction, where the optimum quality factor is obtained. It is evident from the microstructure that as the volume fraction of NaCl increases the grain size increases, resulting in the decrease in dielectric loss and increase in quality factor, which may due to the lesser grain boundaries per unit volume. Penn et al. (1997) also have reported a decrease in dielectric loss with increase in grain size for poly crystalline alumina material. However, Chen et al. reported that the superposition of quality factor of the two initial materials is not considered to be a general model to predict Q value of binary ceramic systems. They calculate the quality factor of binary systems using relative permittivity of individual phases, relative permittivity variation index k of individual phases and quality factor of initial materials (Chen et al., 2017). So a detailed theoretical analysis is required for the prediction of quality factor for composite system. The important parameter, which is connected with the thermal stability of a dielectric material is its temperature coefficient of the resonant frequency (τ_f).The τ_f can be calculated from the temperature coefficient of dielectric constant (τ_ε) and linear thermal expansion coefficient (α_L) using the following formula:

$$\tau_f = -\left[\frac{\tau_\varepsilon}{2} + \alpha_L\right] \tag{8}$$

Here, α_L can be taken as a constant ($\sim +10$ ppm/°C) for all ceramic materials. The measured τ_f value increases linearly from −41 ppm/°C to −112 ppm/°C with increase in x from 0.4 to 0.7, which may due to the large negative temperature coefficient of −171 ppm/°C for NaCl. The theoretical τ_f value of the composite depends on the τ_f values of individual phases as shown in Equation (9),

$$\tau_f = V_1 \tau_{f1} + V_2 \tau_{f2} \tag{9}$$

where V_1 and V_2 represent the volume fractions of individual phases and τ_{f1} and τ_{f2}represent the corresponding temperature coefficient of resonant frequency. According to the above equation, as the volume fraction of NaCl increases the τ_f value also increases, similar to the measured trend.

CONCLUSION

In this work, novel $(1 - x)$NCMVO-xNaCl microwave composite ceramics with high relative densities of >80% were successfully prepared by CSP (200°C, 50 min, and 450 MPa). The results of XRD, SEM, and Raman spectroscopy indicates that there is no chemical reaction between the two phases and only the two characteristic phases of NCMVO and NaCl were present in all composite ceramics. The successful preparation of $(1 - x)$ NCMVO-xNaCl composite ceramics indicates that CSP has great potential in the low temperature fabrication of microwave composite ceramics for 5G enabled technology. The future work aims to tune the properties of the NCMVO ceramics using other additives such as Li_2MoO_4 and K_2MoO_4. Also for practical applications the NaCl based composites should be protected from moisture absorption, which can be done using conformal silicon coating.

DATA AVAILABILITY STATEMENT

The original contributions presented in the study are included in the article/**Supplementary Material**, further inquiries can be directed to the corresponding author.

AUTHOR CONTRIBUTIONS

SG designed the study. RM carried out the experimental part and wrote the manuscript in discussion with SG and SN. All authors contributed to the article and approved the submitted version.

ACKNOWLEDGMENTS

SN is grateful to DST, Govt. of India for financial assistance under the Women Scientists Scheme (WOS-A). We acknowledge KSCSTE-SARD program of the Department of physics, University of Kerala.

SUPPLEMENTARY MATERIAL

The Supplementary Material for this article can be found online at: https://www.frontiersin.org/articles/10.3389/fmats.2021.665033/full#supplementary-material

REFERENCES

Berbano, S. S., Guo, J., Guo, H., Lanagan, M. T., and Randall, C. A. (2017). Cold sintering process of $Li_{1.5}Al_{0.5}Ge_{1.5}$ $(PO_4)_3$ solid electrolyte. *J. Am. Ceram. Soc.* 100, 2123–2135. doi: 10.1111/jace.14727

Bouville, F., and Studart, A. R. (2017). Geologically-inspired strong bulk ceramics made with water at room temperature. *Nat. Commun* 8:14655. doi: 10.1038/ncomms14655

Cava, R. J. (2001). Dielectric materials for applications in microwave communications. *J. Mater. Chem.* 11, 54–62. doi: 10.1039/b003681l

Charoonsuk, T., Sukkha, U., Kolodiazhnyi, T., and Vittiyakom, N. (2018). Enhancing the densification of ceria ceramic at low temperature via the cold sintering assisted two-step sintering process. *Ceram Int.* 44, S54–S57. doi: 10.1016/j.ceramint.2018.08.253

Chen, H., Tang, B., Zhong, C., Yuan, Y., and Zhang, S. (2017). A novel formula for the quality factor calculation for the multiphase microwave dielectric ceramic mixtures. *J. Eur. Ceram. Soc.* 37, 3347–3352. doi: 10.1016/j.jeurceramsoc.2017.04.006

Fang, L., Xiang, F., Su, C., and Zang, H. (2013). A novel low firing microwave dielectric ceramic $NaCa_2Mg_2V_3O_{12}$. *Ceram. Int.* 39, 9779–9783. doi: 10.1016/j.ceramint.2013.05.041

Faouri, S. S., Mostaed, A., Dean, J. S., Wang, D., Sinclair, D. C., Zhang, S., et al. (2019). High quality factor cold sintered Li_2MoO_4-$BaFe_{12}O_{19}$ composites for microwave applications. *Acta Mater.* 166, 202–207. doi: 10.1016/j.actamat.2018.12.057

Fiedziuszko, S. J., Hunter, I. C., Itoh, T., Kobayashi, Y., Nishikawa, T., Stitzer, S. N., et al. (2002). Dielectric materials, devices, and circuits. *IEEE Trans. Microw. Theor. Tech.* 50, 706–720. doi: 10.1109/22.989956

Funahashi, S., Guo, H., Guo, J., Wang, K., Baker, A. L., and Shiratsuyu, K. (2017a). Cold sintering and co-firing of a multilayer device with thermoelectric materials. *J. Am. Ceram. Soc.* 100, 3488–3496. doi: 10.1111/jace.14852

Funahashi, S., Guo, J., Guo, H., Wang, K., Baker, A. L., and Shiratsuyu, K. (2017b). Demonstration of the cold sintering process study for the densification and grain growth of ZnO ceramics. *J. Am. Ceram. Soc.* 100, 546–553. doi: 10.1111/jace.14617

Gonzalez-Julian, J., Neuhaus, K., Bernemann, M., Pereria de silva, J. G., Laptev, A., Brem, M., et al. (2018). Unveiling the mechanisms of cold sintering of ZnO at 250°C by varying applied stress and characterizing grain boundaries by Kelvin probe force microscopy. *Acta Mater.* 144, 116–128.

Green, D. J., Guillon, O., and Rçdel, J. (2008). Constrained sintering: a delicate balance of scales. *J. Eur. Ceram. Soc.* 28, 1451–1466. doi: 10.1016/j.jeurceramsoc.2007.12.012

Guo, J., Baker, A. L., Guo, H., Lanagan, M. T., and Randall, C. A. (2017). Cold sintering process: a new era for ceramic packaging and microwave device development. *J. Am. Ceram. Soc.* 100, 669–677. doi: 10.1111/jace.14603

Guo, J., Berbano, S. S., Guo, H., Baker, A. L., Lanagan, M. T., and Randall, C. A. (2016). Cold sintering process of composites: bridging the processing temperature gap of ceramic and polymer materials. *Adv. Funct. Mater.* 26, 7115–7121. doi: 10.1002/adfm.201602489

Guo, J., Zhou, D., Li, Y., Shao, T., Qi, Z. M., Jin, B. B., et al. (2014a). Structure-property relationships of novel microwave dielectric ceramics with low sintering temperatures: $(Na_{0.5}xBi_{0.5}xCa_{1-x})$ MoO_4. *Dalton Trans.* 43, 11888–11896. doi: 10.1039/C4DT00838C

Guo, J., Zhou, D., Zou, S. L., Wang, H., Pang, L. X., and Yao, X. (2014b). Microwave dielectric ceramics Li_2MO_4-TiO_2 (M=Mo,W) with low sintering temperatures. *J. Am. Ceram. Soc.* 97:1819. doi: 10.1111/jace.12821

Hong, W. B., Li, L., Cao, M., and Chen, X. M. (2018). Plastic deformation and effects of water in room-temperature cold sintering of NaCl microwave dielectric ceramics. *J. Am. Ceram. Soc.* 101, 4038–4043. doi: 10.1111/jace.15572

Induja, I. J., and Sebastian, M. T. (2017). Microwave dielectric properties of mineral sillimanite obtained by conventional and cold sintering process. *J. Eur. Ceram. Soc.* 37, 2143–2147. doi: 10.1016/j.jeurceramsoc.2017.01.007

Induja, I. J., and Sebastian, M. T. (2018). Microwave dielectric properties of cold sintered Al_2O_3–NaCl composite. *Mater. Lett.* 211, 55–57. doi: 10.1016/j.matlet.2017.09.083

Ji, Y., Song, K., Luo, X., Liu, B., Barzegar Bafrooei, H., and Wang, D. (2019). Microwave dielectric properties of (1-x) Li_2MoO_4–xMg_2SiO_4 composite ceramics fabricated by cold sintering process. *Front. Mater.* 6:256. doi: 10.3389/fmats.2019.00256

Kahari, H., Ramachandran, P., Juuti, J., and Jantunen, H. (2017). Room temperature densified Li_2MoO_4 ceramic patch antenna and the effect of humidity. *J. Appl. Ceram.Technol.* 14:50. doi: 10.1111/ijac.12615

Kahari, H., Teirikangas, M., Juuti, J., and Jantunen, H. (2014). Dielectric properties of lithium molybdate ceramic fabricated at room temperature. *J. Am. Ceram. Soc.* 97, 3378–3379. doi: 10.1111/jace.13277

Kähäri, H., Teirikangas, M., Juuti, J., and Jantunen, H. (2016). Room-temperature fabrication of microwave dielectric Li_2MoO_4-TiO_2 composite ceramics. *Ceram. Int.* 42, 11442–11446. doi: 10.1016/j.ceramint.2016.04.081

Koningstein, J. A., and Mortensen, O. S. (1968). Laser-excited phonon Raman spectrum of garnets. *J. Mol. Spectrosc.* 27, 343–350. doi: 10.1016/0022-2852(68)90043-X

Lee, W., Lyon, C. K., Seo, J.-H., Lopez-Hallman, R., Leng, Y., Wang, C.-Y., et al. (2019). Ceramic–salt composite electrolytes from cold sintering. *Adv. Electron. Mater.* 29:1807872.

Leng, H., Huang, J., Nie, J., and Luo, J. (2018). Cold sintering and ionic conductivities of $Na_{3.256}Mg_{0.128}Zr_{1.872}Si_2PO_{12}$ solid electrolytes. *J. Power Sources* 391, 170–179. doi: 10.1016/j.jpowsour.2018.04.067

Maria, J. P., Kang, X., Floyd, R. D., Dickey, E. C., Guo, H., Guo, J., et al. (2017). Cold sintering: current status and prospects. *J. Mater. Res.* 32, 3205–3218. doi: 10.1557/jmr.2017.262

Moore, R. K., White, W. B., and Long, T. V. (1971). Vibrational spectra of the common silicates. *I. Garnets. Am. Miner.* 56, 54–71.

Ndayishimiye, A., Buf, S., Dourges, M., Largeteau, A., Prakasom, M., Mornet, S., et al. (2018a). Design of 0–3 type nano composites using hydrothermal sintering. *Scr. Mater.* 148, 15–19. doi: 10.1016/j.scriptamat.2018.01.013

Ndayishimiye, A., Largeteau, A., Prakasam, M., Dourges, M. A., and Goglio, G. (2018b). Low temperature hydrothermal sintering process for the quasi-complete densification of nanometric α -quartz. *Scr. Mater.* 145, 118–121.

Ohsato, H. (2012). Functional advances of microwave dielectric for next generation. *Ceram. Int.* 38, S141–S146. doi: 10.1016/j.ceramint.2011.04.068

Penn, S. J., Alfrod, N. M., Templeton, A., Wang, X., Xu, M., Reece, M., et al. (1997). Effect of porosity and grain size on the microwave dielectric properties of sintered alumina. *J. Am. Ceram. Soc.* 80:1885. doi: 10.1111/j.1151-2916.1997.tb03066.x

Rakhi, M., and Subodh, G. (2020). Crystal structure, phonon modes, and bond characteristics of $AgPb_2B_2V_3O_{12}$ (B = Mg, Zn) microwave ceramics. *J. Am. Ceram. Soc.* 103, 3157–3167. doi: 10.1111/jace.16991

Randall, C. A., Guo, J., Guo, H., Baker, A., and Lanagan, M. T. (2017). *Cold Sintering Ceramics and Composites.* U.S. Provisional Patent Application No 20170088471. University Park, PA: The Penn State Research Foundation.

Reaney, I. M., and Iddles, D. (2006). Microwave dielectric ceramics for resonators and filters in mobile phone networks. *J. Am. Ceram. Soc.* 89, 2063–2072. doi: 10.1111/j.1551-2916.2006.01025.x

Santha, N., Rakhi, M., and Subodh, G. (2020). Fabrication of high quality factor cold sintered $MgTiO_3$–NaCl microwave ceramic composites. *Material Chem. Phys.* 255:123636. doi: 10.1016/j.matchemphys.2020.123636

Sebastian, M. T., Ubic, R., and Jantunen, H. (2015). Low-loss dielectric ceramic materials and their properties. *Int. Mater. Rev.* 60, 392–412. doi: 10.1179/1743280415Y.0000000007

Seo, J. H., Guo, J., Guo, H., Verlinde, K., Baba Heidery, D. S., Rajagopalan, R., et al. (2017). Cold sintering of a Li-ion cathode: $LiFePO_4$-composite with high volumetric capacity. *Ceram. Int.* 43, 15370–15374. doi: 10.1016/j.ceramint.2017.08.077

Sibi, N., Rajan, A., and Subodh, G. (2020). Garnet mineral-based composites through cold sintering process: microstructure and dielectric properties. *J. Eur. Ceram. Soc.* 40, 371–375. doi: 10.1016/j.jeurceramsoc.2019.09.012

Väätäjä, M., Kähäri, H., Juuti, J., and Jantunen, H. (2017). Li_2MoO_4-based composite ceramics fabricated from temperature-and atmosphere-sensitive MnZn ferrite at room temperature. *J. Am. Ceram. Soc.* 100, 3626–3635. doi: 10.1111/jace.14914

Väätäjä, M., Kähäri, H., Ohenoja, K., Sobocinski, M., Juuti, J., and Jantunen, H. (2018). 3D printed dielectric ceramics without sintering stage. *Sci. Rep.* 8:15955. doi: 10.1038/s41598-018-34408-5

Wang, D., Guo, H., Morandi, C. S., Randall, C. A., and Mckinstry, S. T. (2018a). Cold sintering and electrical characterization of lead zirconate titanate piezoelectric ceramics. *APL Mater*. 6:16101. doi: 10.1063/1.5004420

Wang, D., Li, L., Jiang, J., Lu, Z., Wang, G., and Song, K. (2021). Cold sintering of microwave ceramics and devices. *J. Mater. Res.* 36, 333–349. doi: 10.1557/s43578-020-00029-w

Wang, D., Zhang, S., Wang, G., Vardaxoglou, Y., Whittow, W., Cadman, D., et al. (2020). Cold sintered $CaTiO_3$-K_2MoO_4 microwave dielectric ceramics for integrated microstrip patch antennas. *Appl. Mater. Today* 18:100519.

Wang, D., Zhang, S., Zhou, D., Song, K., Feteira, A., Vardaxoglou, Y., et al. (2019a). Temperature stable cold sintered $(Bi_{0.95}Li_{0.05})$ $(V_{0.9}Mo_{0.1})$ O_4-$Na_2Mo_2O_7$ microwave dielectric composites. *Materials* 12:1370. doi: 10.3390/ma12091370

Wang, D., Zhou, D., Song, K., Feteira, A., Randall, C. A., and Reaney, I. M. (2019b). Cold sintered C0G multilayer ceramic capacitors. *Adv. Electron. Mater.* 5:1900025.

Wang, D., Zhou, D., Zhang, S., Vardaxoglou, Y., Whittow, W. G., Cadman, D., et al. (2018b). Cold-sintered temperature stable $Na_{0.5}Bi_{0.5}MoO_4$-Li_2MoO_4 microwave composite ceramics. *ACS Sustain. Chem. Eng.* 6, 2438–2444. doi: 10.1021/acssuschemeng.7b03889

White, W. B., and Keramidas, V. G. (1971). Raman spectra of yttrium iron garnet and two vanadium garnets. *J. Am. Ceram. Soc.* 54, 472–473. doi: 10.1111/j.1151-2916.1971.tb12392.x

Yoon, S. H., Kim, D. W., Cho, S. Y., and Hong, K. S. (2006). Investigation of the relations between structure and microwave dielectric properties of divalent metal tungstate compounds. *J. Eur. Ceram. Soc.* 26, 2051–2054. doi: 10.1016/j.jeurceramsoc.2005.09.058

Yu, T., Cheng, J., Li, L., Sun, B., Bao, X., and Zhang, H. (2019). Current understanding and applications of the cold sintering process. *Front. Chem. Sci. Eng.* 13:654–664. doi: 10.1007/s11705-019-1832-1

Zhou, D., Pang, L., Wang, D., and Reaney, I. M. (2018). $BiVO_4$ based high k microwave dielectric materials: a review. *J. Mater. Chem. C.* 6, 9290–9313. doi: 10.1039/C8TC02260G

Zhou, D., Randall, C. A., Pang, L. X., Hong, W., Jing, G., and Gao, Q. Z. (2011). Microwave dielectric properties of Li_2WO_4 ceramic with ultra-low sintering temperature. *J. Am. Ceram. Soc.* 94, 348–350. doi: 10.1111/j.1551-2916.2010.04312.x

Conflict of Interest: The authors declare that the research was conducted in the absence of any commercial or financial relationships that could be construed as a potential conflict of interest.